LAWRENCE
LIVERMORE
NATIONAL
LABORATORY

LLNL-JRNL-579933

High pressure-temperature phase diagram and equation of state of beryllium

A. Lazicki, A. Dewaele, P. Loubeyre, M. Mezouar

September 10, 2012

Physical Review B

Disclaimer

High pressure-temperature phase diagram and equation of state of beryllium

Amy Lazicki
CEA, DAM, DIF, 91297 Arpajon Cedex, France and Lawrence Livermore National Laboratory, Livermore, CA 94551 USA

Agnès Dewaele and Paul Loubeyre
CEA, DAM, DIF, 91297 Arpajon Cedex, France

Mohamed Mezouar
European Synchrotron Radiation Facility, BP 220, F-38043 Grenoble Cedex, France

X-ray diffraction of beryllium in a laser heated diamond anvil cell provides new experimental insight into its behavior at high pressure and temperature. We measure the cold compression of Be in helium and NaCl pressure media up 192 GPa, and its thermal expansion up to 82 GPa and 2630K. The new measurements form a $P-V-T$ data set which is fit by the Vinet-Deybe form to establish a Be experimental equation of state. We compare the results to several theoretical models. The crystal structure of Be is determined up to 200 GPa and 4000K; no evidence for the predicted high-temperature transition to a cubic phase is found. Finally, the maximum temperature stability of the solid phase along isobaric heating ramps gives a lower bound for the melting curve.

Properties of beryllium at high temperature and pressure are important primarily because its light weight and low density coupled with high strength and high thermal conductivity make Be very useful for the defense, aerospace and nuclear power industries. Of particular recent interest is its potential as a capsule material for inertial confinement fusion (ICF)[1]. High laser ablation rate, high thermal conductivity and stability against Rayleigh-Taylor growth[2] make (doped) Be potentially a better option than the currently employed plastic capsule material. The initial laser pulse in the ICF design will bring the Be capsule to pressures on the order of 2 Mbar and temperatures of 4000 K[3], the thermodynamic domain covered in this study. The response of the capsule to this initial pulse is an important constraint for theoretical models which attempt to describe the much more extreme conditions achieved during subsequent pulses.

As a subject of theoretical studies, Be has received a lot of attention because it represents a special case among other divalent metals with c/a much less than ideal, an exceptionally high Debye temperature and small Poissons ratio. Also, under pressure Be is predicted to exhibit multiple solid phases which are very close in energy, with their relative stability affected by anharmonic effects at high T[4–7]. There have been some experimental reports of a new high-temperature phase (β-Be): body-centered cubic (bcc)[8,9] or hexagonal[11], which was later re-interpreted[12], suggesting a smaller 4-atom orthorhombic (distorted hcp) unit cell instead. The stability domain of the β-Be phase was reported to extend from 1530 to 1560 K (the melting point)[8] at ambient pressure, and from indirect evidence in a large-volume press apparatus, it was inferred that the Clapeyron slope of the α to β-Be transition was negative[10]. A tentative stability domain of β-Be, based on these observations, is represented Figure 1. Theoretically, however, a low-pressure pocket of β-Be cannot be stabilized without strong anharmonic effects, as it is dynamically unstable at low pressure. Instead, a bcc phase is predicted to appear close to the melting line above 100[5,6,13,14]. Recent experimental studies have seen no evidence for the bcc phase, either at low pressure, or up to 200 GPa at ambient temperature[15,16], or between 15 and 50 GPa at temperatures up to 2000K[17].

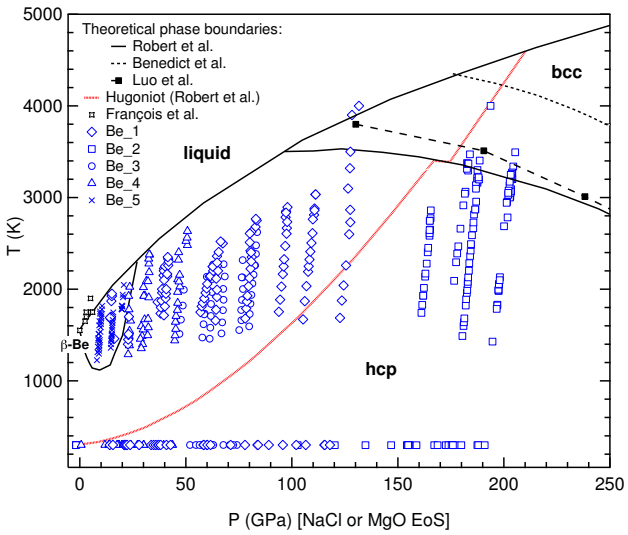

FIG. 1: (Color online) The data points in P-T space, as blue symbols, at which X-ray diffraction patterns have been collected. There was no sign of a bcc or β-Be phase in any of the diffraction patterns. The lines correspond to the phase boundaries predicted by theoretical studies[4–6] , and the model Hugoniot[5].

High temperature measurements of Be in the literature have so far been limited to the very low pressure regime[8,10,18,20]. Various experimental[18,19] and theoretical[4–7] studies have reported values for thermal expansion

The goals of this study were: to measure an equation

of state of Be to high precision, combining the cold compression curve and the thermal expansion; to investigate the evolution of the melting curve at very high pressure; to confirm the stability field of β-Be; and to search for the predicted bcc-Be at very high pressure.

I. EXPERIMENTAL METHODS

Three runs were dedicated to the accurate measurement of the equation of state (EoS) of beryllium from synchrotron single crystal X-ray diffraction (XRD), on the ID30 beamline at ESRF (Grenoble, France). Small single crystals (≤ 4 μm) were loaded in membrane diamond anvil cells, with helium as a pressure transmitting medium. The thickness of the sample chamber was always larger than the dimension of the crystal. The experiments have been carried out using single crystal energy dispersive XRD. The same technique had been used to measure with high accuracy the equation of state of low-Z system in the 100 GPa range[21]. An average of 5 reflections were measured in each run; relative uncertainty on the lattice parameter was of the order of 4×10^{-4}Å. The pressure was estimated from the luminescence of a small ruby ball (about 3 μm in diameter) and its quasi-hydrostatic revised calibration[22,41].

For two of the heating runs (Be_1 and Be_2), pressed pellets of Be were loaded between plates of NaCl in diamond cells with beveled diamond culets of 150×300 μm and 70×300 μm in diameter. The NaCl was necessary for thermal insulation and to prevent chemical reaction between beryllium and diamond, which form beryllium carbide at high temperature. No reaction between Be and NaCl was observed. In one of these cells (Be_2), the diamonds had pits in their tips of a depth of $\simeq$3 μm, to maximize thickness of the sample and the NaCl thermal insulation. Pressure was determined from the lattice parameters of NaCl. The cold compression curve of this calibrant has been obtained by merging most recent P-V measurements[24,25]. The following parameters of the B2-NaCl EoS have been obtained: V_0=45.27 Å^3/formula unit, K_0=15.2 GPa, and K_0'=6.07, with a Rydberg-Vinet EoS[31]. The thermal pressure of NaCl has been taken from Ref. 26, which uses a Mie-Grüneisen-Debye approach and is based on a large body of experimental data. Because of strong temperature gradients away from the heated beryllium, the pressure determination at high temperature has a large uncertainty.

For the remaining two heating runs (Be_3 and Be_4), the thin Be plates were pressed together with $\simeq$1 μm-thick layers of MgO, in close thermal contact with the Be and insulated from the diamonds with plates of NaCl. With this sample assembly, the temperature of the pressure gauge MgO is expected to be close to the temperature of the Be sample. A more accurate pressure determination at high temperature was then made based on the high P-T equation of state of MgO[41].

Laser heating was performed at the ID27 beamline at the ESRF, with setup and methods described elsewhere[27]. Temperature was determined from spectral radiometry measurements[28], with an average uncertaintly of 50K.

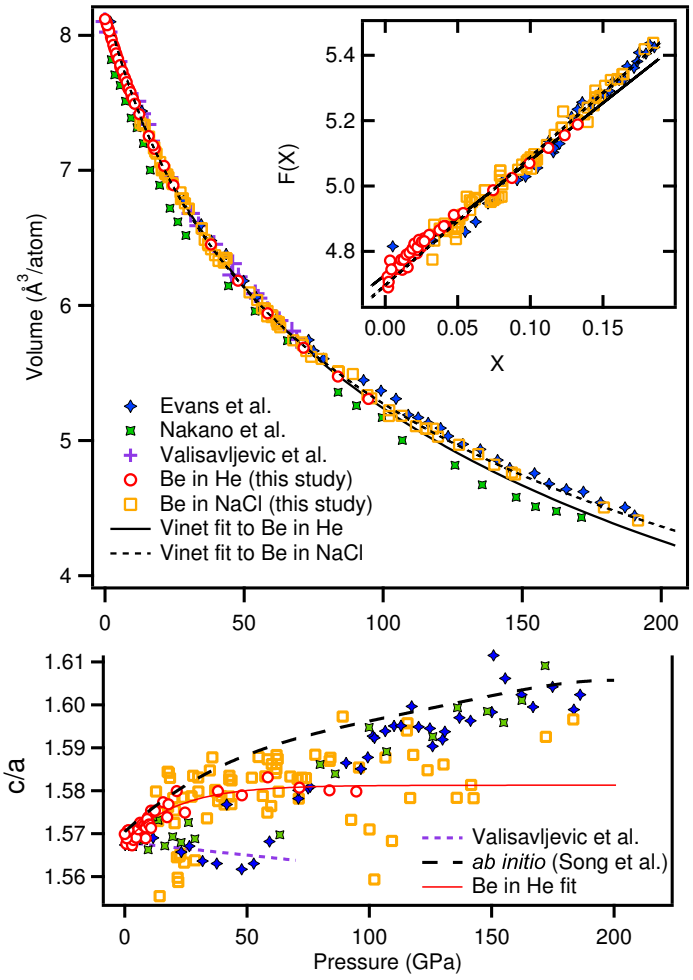

FIG. 2: (Color online) Upper panel: summary of 300K isotherm measured in this study, compared with past experimental results. Error bars associated with measurement uncertainties for the data collected in this study do not exceed the size of the data points. The dispersion of the data is due to the non-hydrostatic stress. The data of Evans et al.[15] (Be contained in a He medium) are corrected for the new Au pressure scale, and those of Nakano et al.[16] and Velisavljevic et al.[29] (no pressure medium) for the new ruby scale. Inset: Normalized stress vs. Eulerian strain terms, from which the bulk modulus K_0 and pressure derivative K_0' were calculated. Lower panel: evolution of the c/a ratio for these various studies (and an *ab inito* result[7]). The scatter of the data gives an indication of the degree of uncertainty. The c/a ratio at high temperature found during the heating cycles of the Be in NaCl showed no clear trend in temperature.

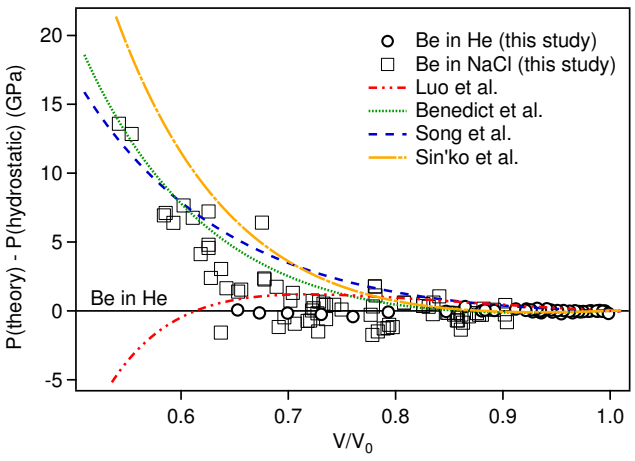

FIG. 3: (Color online) Comparison of experimental data to various theoretical models. All curves and data show the deviation of the theoretical EoS from the optimally hydrostatic EoS determined in this study from the compression of single crystal Be in the He medium.

II. COLD COMPRESSION CURVE

Ambient temperature equation of state (EoS) measurements are reported in Figure 2 and data is given in Table I. The volume determination from the single-crystal Be samples compressed in a He medium up to 93 GPa yields the P-V points with the lowest scatter. Nonhydrostatic stresses were negligible, as evidenced by the lack of broadening or distortion of single crystal spots at high pressure. No evidence of any distorsion of the hexagonal close packed lattice[11] has been observed, confirming the conclusions of most recent x-ray diffraction studies of beryllium[15,16,29]. The lattice parameters obtained at each pressure point, for the three experimental runs, are presented in table I.

Samples of Be compressed up to nearly 2 Mbars for the purpose of laser heating were contained in the less hydrostatic NaCl medium. The crystalline phase of beryllium remained hcp up to the maximum pressure reached. The ambient temperature volume measurements from these runs are also shown in Fig. 2.

To provide useful physical parameters (namely volume V_0, bulk modulus K_0, and its pressure derivative K_0', under ambient conditions) the $P-V$ data points have been fitted by an EoS functional form. We used the Rydberg-Vinet EoS[31], that expresses the pressure as a function of $X = (V/V_0)^{1/3}$ through:

$$P = 3K_0X^{-2}(1-X)\exp(1.5(K_0'-1)(1-X)). \quad (1)$$

V_0 is determined from a fitting of the above equation to $P-V$ data from the single-crystal Be in He and then fixed at this value for the fitting to the data from Be in NaCl, since the latter does not extend to sufficiently low pressure for a reliable fitted V_0 value. The equation may be reformulated as a normalized stress term: $ln[H(X)] = \ln\left[\frac{PX^2}{3(1-X)}\right]$ and an Eulerian strain term: $(1-X)$. The results are plotted in the inset of Fig. 2. The data follow a linear trend, the slope of which yields the pressure derivative of the bulk modulus K_0', and the y-intercept the bulk modulus K_0. Fitting parameters are listed in Table II.

Also in Fig. 2 are shown most recent experimental results, for comparison. The data collected by Evans et al. were from samples compressed in He as well, with pressure determined from the calibrated equation of state of Au[40]. We have corrected these data points using a more accurate Au EoS[41,42], resulting in a shift relative to the published results.

It can be seen in Fig. 2 that the Be EoS measured in the less hydrostatic NaCl pressure medium (even laser-annealed, as in this case) is slightly stiffer than the extension of the one measured in a He pressure medium, as is well known when nonhydrostatic stresses are present in conventional diffraction geometry in diamond anvil cells. The EoS of Evans et al. is stiffer than both the EoS measured in this study (though the difference from our data in NaCl is very low). The appearance of less hydrostatic conditions in the data set of Evans et al. could be evidence that the Be sample was bridging the two diamond anvils and thus being uniaxially compressed. High precision measurements need to be extended to higher pressure to confirm this.

Also shown for comparison are the results of Nakano et al.[16], and Velisavljevic et al.[29], both compressed without pressure medium, using ruby fluorescence as the pressure calibrant. The data have been corrected for the new ruby scale[41]. Ref. 29 data agree surprisingly well with the more hydrostatic compression studies.

The evolution of the c/a ratio is shown in the lower panel of Fig. 2. At ambient pressure it takes on an unusually low value which increases under pressure but seems to saturate around 1.59. This variation from the ideal value of 1.633 can be explained in terms of band structure effects. The small c/a ratio has the effect of keeping a set of very flat p-bands below the Fermi level, significantly reducing the total band energy[30] . The degree of scatter in the experimental data gives a good approximation of the average uncertainty for any given data point. The scatter is smallest for the current data obtained with single crystal XRD in helium medium, and rather large for the the current data obtained in NaCl medium. This may be explained by single crystal diffraction peaks coming from crystallites with slightly different stress conditions. For the highest precision measurements, the c/a ratio increases approximately linearly up to about 30 GPa, after which it increases only slightly. The different and irregular behavior of c/a in Ref. 15 may be a sign of a change of the stress distribution around 60 GPa in the powdered sample.

The cold compression curve is a very sensitive test of the exchange-correlation functionals that best describe the condensed matter properties of an element. Model predictions for the Be equation of state are shown in

TABLE I: Lattice parameters of Be in the hexagonal closed packed phase (a and c) at ambient T. P is in GPa, a and c in Å, V in Å^3/formula unit. Be in He: the pressure in the diamond-anvil cell chamber is measured by the ruby luminescence technique with the calibration from Ref. 26. Three experimental runs have been performed: $0.65 \leq P \leq 21.2$ GPa; $0 \leq P \leq 94.7$ GPa; $0.55 \leq P \leq 10.7$ GPa. Be in NaCl: the pressure is measured using NaCl volume V (see text). Four experimental runs have been performed.

Be in He						Be in NaCl							
P	a	c	P	a	c	MgO V	P	a	c	NaCl V	P	a	c
0.65	2.284	3.580	0.54	2.284	3.585	17.428	12.8	2.208	3.489	33.563	14.3	2.217	3.448
1.36	2.279	3.575	1.19	2.279	3.580	17.353	13.7	2.208	3.473	32.967	15.9	2.199	3.463
2.13	2.273	3.570	2.38	2.272	3.564	17.038	17.7	2.190	3.452	31.204	21.4	2.179	3.409
3.28	2.266	3.556	2.98	2.269	3.556	16.886	19.8	2.178	3.438	31.136	21.6	2.178	3.397
4.18	2.260	3.548	3.51	2.265	3.553	16.978	18.5	2.182	3.455	31.067	21.8	2.178	3.394
5.53	2.252	3.535	4.02	2.262	3.550	17.012	18.1	2.183	3.459	30.911	22.4	2.175	3.403
6.83	2.244	3.528	4.65	2.258	3.544	17.051	17.5	2.185	3.463	30.803	22.8	2.172	3.401
8.29	2.236	3.515	5.48	2.253	3.539	16.845	20.4	2.174	3.419	30.413	24.3	2.168	3.389
9.60	2.229	3.508	6.25	2.248	3.535	16.840	20.5	2.175	3.426	29.387	28.7	2.153	3.367
10.7	2.223	3.503	7.17	2.243	3.527	16.595	24.1	2.162	3.412	27.063	33.6	2.128	3.348
12.3	2.215	3.490	7.80	2.240	3.521	16.348	28.0	2.148	3.401	26.858	34.8	2.123	3.365
15.7	2.198	3.467	8.55	2.236	3.513	16.398	27.2	2.155	3.401	26.680	35.9	2.113	3.355
17.8	2.189	3.451	9.19	2.232	3.512	16.391	27.3	2.149	3.393	26.500	37.0	2.113	3.339
21.2	2.174	3.435	9.96	2.228	3.503	16.219	30.1	2.141	3.383	26.480	37.2	2.112	3.337
			10.7	2.225	3.496	16.224	30.1	2.140	3.387	26.315	38.1	2.110	3.329
8.59	2.236	3.509	1.49	2.277	3.577	15.703	39.5	2.104	3.322	25.915	40.8	2.101	3.312
17.3	2.193	3.451	0.79	2.282	3.581	15.502	43.6	2.103	3.316	25.643	42.7	2.099	3.313
24.6	2.262	3.405	0.0	2.286	3.589	15.5	43.6	2.100	3.324	23.831	58.3	2.055	3.237
38.1	2.113	3.338								23.674	59.9	2.054	3.238
47.9	2.083	3.290				15.551	42.7	2.099	3.321	23.814	58.5	2.054	3.261
58.4	2.054	3.252				15.546	42.8	2.100	3.326	23.651	60.1	2.051	3.253
71.4	2.025	3.202				15.126	52.0	2.072	3.280	23.506	61.6	2.047	3.243
83.7	2.000	3.160				15.008	54.7	2.063	3.276	22.683	71.1	2.029	3.202
94.7	1.980	3.128				14.896	57.4	2.058	3.259	22.166	77.9	2.012	3.196
						14.937	56.4	2.060	3.253	21.755	83.8	2.002	3.177
						14.716	62.0	2.044	3.239	21.736	84.0	2.001	3.177
						14.696	62.5	2.045	3.246	21.407	89.1	1.995	3.187
						14.714	62.1	2.044	3.246	21.006	95.7	1.978	3.136
						14.680	62.9	2.044	3.229	20.652	102.0	1.973	3.076
						14.396	70.7	2.029	3.212	20.411	106.6	1.961	3.113
						14.504	67.7	2.031	3.215	19.977	115.3	1.946	3.102
						14.280	74.1	2.017	3.192	19.968	115.5	1.946	3.105
						14.338	72.4	2.0216	3.200	19.856	117.9	1.949	3.095
										21.089	94.3	1.986	3.124
										20.643	102.2	1.973	3.099
										20.149	111.8	1.960	3.072
										19.776	119.7	1.945	3.070
										19.442	127.3	1.935	3.066
										19.158	134.2	1.925	3.053
										18.932	140.0	1.918	3.027
										18.698	146.3	1.909	3.019
										18.656	147.4	1.908	3.012
										17.631	179.4	1.869	2.977
										17.291	191.6	1.854	2.961

TABLE II: Rydberg-Vinet[31] equation of state fitting parameters for the current data, compared to previous X-ray diffraction, ultrasonic and shock measurements, and to theoretical predictions. The numbers in bold font have been fixed during the fit. ZPV: zero-point vibrations; LDA: Local Density Approximation; GGA: Generalized Global Approximation; PAW: Projector Augmented Wave; FPLMTO: Full Potential Linear Muffin Tin Orbitals; Pseudo: pseudopotential

	P range (GPa)	V_0 (Å^3/atom)	K_0 (GPa)	K_0'
This study, Be in He[a]	0-93	8.133(5)	114(1)	3.27(5)
This study, Be in NaCl[a]	12-192	**8.133**	110(2)	3.62(9)
Evans et al., diffraction[15 b]	1-190		115(1)	3.53(3)
Nakano et al., diffraction[16 b]	1-171		100	3.72
Velisavljevic et al., diffraction[29 c]	0-66		100.8	4.388
ultrasonic[32–35]			112(1)[e]	4.6 [f]
Luo et al.[4], Pseudo-LDA (PZ[36]) (300K) with ZPV[b]		7.910	118	3.21
Benedict et al.[6,43], Pseudo or FPLMTO-GGA (PBE[37]) (300K) without ZPV[a]		7.867	111.6	3.63
Song et al.[7], PAW-GGA (PBE[37]) (293K) with ZPV[d]		8.145	116	3.45
Sin'ko et al.[13], FPLMTO-GGA (Hedin-Lundqvist[38,39]) (298K) with ZPV[d]		8.067	114	4.34

[a]Rydberg-Vinet EoS
[b]3rd order Birch-Murnaghan EoS
[c]AP2 EoS
[d]EoS form not reported
[e]Isothermal bulk modulus deduced from single crystal elastic constants. The adiabatic bulk modulus $K_S = (C_{33}(C_{11} + C_{123} - 2C_{13}^2)/(C_{11} + C_{12} - 4C_{13} + 2C_{33})$. The adiabatic to isothermal correction has been done.
[f]from[33]. No adiabatic to isothermal correction has been carried out.

Figure 3. The 300K *ab initio* results of Benedict[43] are slightly modified from those presented in Ref. 6, to improve the fit to the GGA-DFT results discussed in that paper. When zero-point vibrations are included, the equilibrium volume obtained with generalized-gradient approximation, GGA, is within 1% of experimental V_0 (Table II). *Ab initio* results are presented in terms of compression $V/V_{0\,ai}$ rather than absolute volume to correct for differing V_0 values. Corrected this way, *ab initio* predictions from Ref. 43 and Ref. 7 follow very closely the equation of state determined from Be compressed in NaCl. Both calculations have been performed with the same approximation of exchange-correlation energy (GGA with the PBE functional). The EoS predicted by Sin'ko et al.[13] deviates more significantly from experimental data; it has been obtained within GGA but with a different functional. Luo et al.[4] calculations have been performed within the local density approximation, LDA, and exhibit a different trend. All EoS predicted by density functional theory-GGA are stiffer than the Be in He EoS, a trend which is similar to what has already been noticed for several metals with PAW-GGA calculations[44].

III. STABILITY OF THE BCC PHASE

Thin samples of Be were laser heated directly for the high temperature studies. Well insulated from the diamond surfaces, the Be couples very well with the laser radiation and heating is stable. At high temperature, the

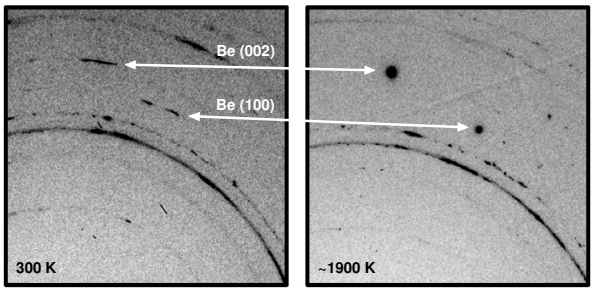

FIG. 4: X-ray diffraction patterns showing ambient T and heated beryllium diffraction peaks at ∼30 GPa.

Be begins to recrystallize, and only isolated single-crystal spots may be seen on the image plate (Fig. 4); generally 2 or 3 spots per peak class. Upon further raising of the temperature, the azimuthal positions of the single-crystal spots on the image plate begin to shift continuously (see below for further discussion). The P-T paths followed in this study are shown in Fig. 1. We observed that up to the maximum pressure and temperature reached (205 GPa and ∼4000K), beryllium remained in the hcp phase. The fact that new single crystal hcp peaks were often appearing in the diffraction pattern, proving a recrystallization of the hcp phase, suggests that this phase was not metastably preserved but the actual thermodynamically stable phase in the P-T range of this study. This means

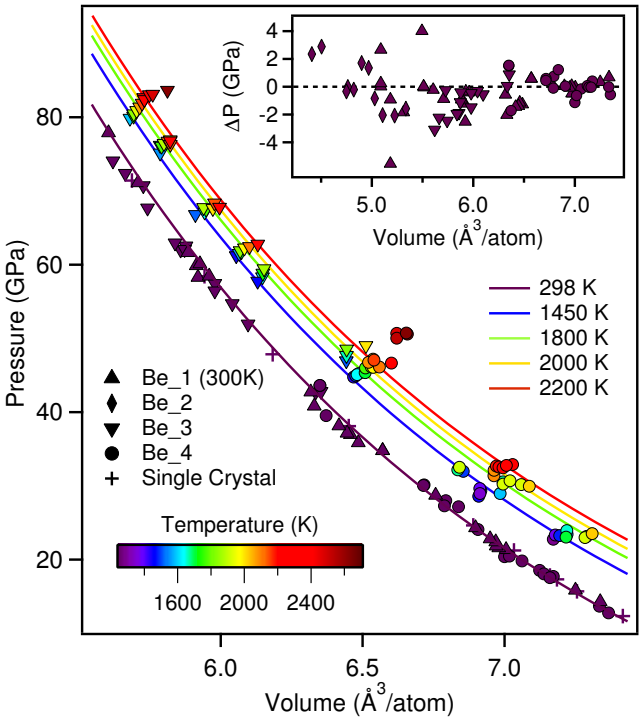

FIG. 5: (Color online) High temperature equation of state. Inset: Deviation of experimental data from equation of state fit for Be in NaCl.

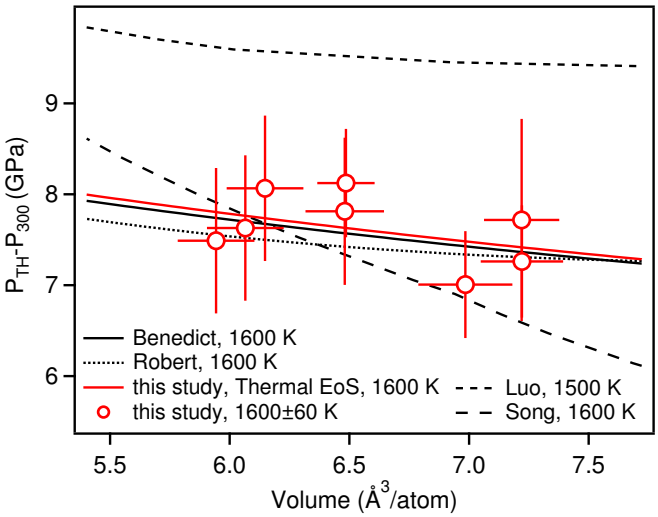

FIG. 6: (Color online) Thermal pressure at 1600K from the various theoretical predictions[4–7] compared to measurements made in this study.

that the bcc phase should become stable at more extreme conditions than predicted by two theoretical studies[4,5].

β-Be was not observed in the moderate pressure runs, *e.g.* down to 8 GPa and 1225 K, which is in the stability pocket of β-Be inferred from a previous experimental report[10]. The stability field of β-Be is probably much narrower than previously thought and on the basis of our measurements, a positive α-Be to β-Be Clapeyron slope is possible. The effect of impurities on the stability of β-Be is debated in the literature[8] and might be the cause of the apparent discrepancy between our observations and a previous report[10].

IV. THERMAL EXPANSION UNDER PRESSURE

The data presented in this section have been obtained with Be_3 and Be_4 samples, for which the temperature was measured by pyrometry and pressure using MgO volume with Ref. 41 EoS. The P-V-T data points are listed in Table III.

Several theoretical models have been used to predict the thermal expansion of Be in the literature[4–7]. These models express the free energy within the Mie-Grüneisen approximation as $F(V,T) = F_0(V) + F_i(V,T) + F_e(V,T)$, where $F_0(V)$ is the static lattice component, $F_i(V,T)$ represents the contribution from ionic motion and $F_e(V,T)$ from excited electrons. The electron thermal contributions have been determined to be negligible compared to the ion-thermal component in the range of interest of this study ($T \leq 5000$K)[6]. Three of the models use the quasiharmonic (QHA) approximation to represent the ion thermal contribution: Luo et al.[4] (hereafter named "Luo"), Benedict et al.[6] (hereafter named "Benedict") and Robert et al.[5] (hereafter named "Robert"), each formulated it slightly differently. The volume derivative of the free energy yields the thermal contribution to the pressure. In the model of Benedict the ion thermal contribution to the pressure is as follows:

$$P_i(V,T) = 9k_BT\left(\frac{B}{V}+A\right)\left[\frac{\theta}{8T}+\frac{1}{3}D\left(\frac{\theta}{T}\right)\right] \qquad (2)$$

where $D(\theta/T)$ is the Debye function and θ is defined as:

$$\theta(V) = \theta^{(0)}\left(\frac{V}{V_{ref}}\right)^{-B}\exp[A(V_{ref}-V)]. \qquad (3)$$

This corresponds to the following expression for the Grüneisen parameter: $\gamma = A \times V + B$. $\theta^{(0)}$, A and B have been calculated using the phonon density of states calculated with the same *ab initio* techniques and approximations as the cold compression curve (GGA-PBE). The Luo study[4] defines the free energy similarly, but does not report an analytic form for the Debye temperature. The fourth model published by Song et al.[7], hereafter called "Song", uses a mean-field potential (MFP) approach, for which detailed fitting parameters are not given. The curves presented here are based on their plots.

We have fitted the experimental P-V points with the form used by Benedict, fixing $\theta^{(0)}$ and V_{ref} to literature values: 949K from thermodynamic measurements[19] and 8.133 Å^3/atom, respectively. The fitted A and B pa-

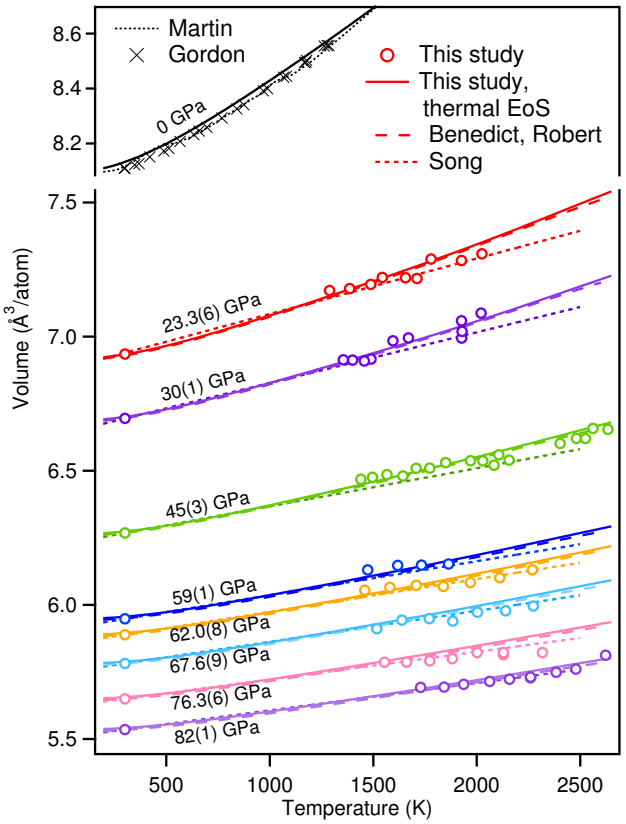

FIG. 7: (Color online) Volumetric thermal expansion, compared with theoretical models[5–7] and previous ambient pressure results[8,20]

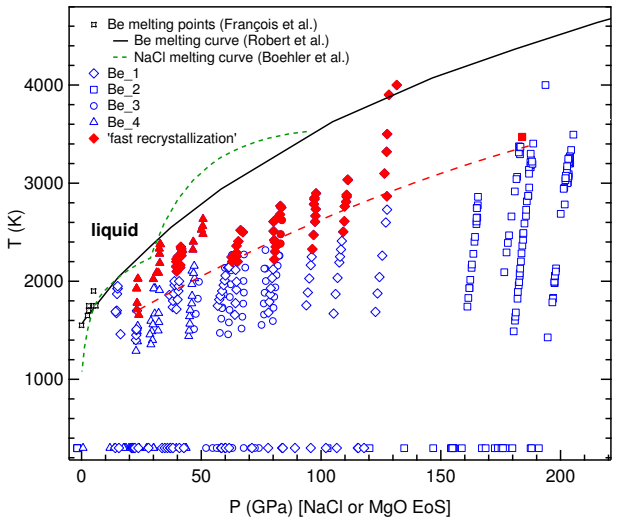

FIG. 8: (Color online) P-T conditions at which we see fast recrystallization of the beryllium samples. The red dashed line is a guide to the eyes, which indicates the approximate temperature of the sample's fast recrystallization onset. The melting line predicted by Robert *et al.*[5] and measured by Francois *et al.* are also plotted, along with melting line of the NaCl pressure medium according to Ref. 48.

rameters are: A= 0.079 Å^{-3} and B = 0.542. The corresponding curves are shown in Fig. 5. This is not a unique solution, because the data are too sparse and scattered for a well-constrained fit. It can be noted however that the fitting parameters are very close to those of Benedict (A, B, $\theta^{(0)}$ and V_{ref} being respectively 0.081 Å^{-3}, 0.515, 982.8 K and 7.75 Å^3/atom).

The thermal pressure predicted by the various models[4–7] at $\sim$ 1600 K is shown in Fig. 6, compared to experimental results. The Song model[7] and two of the QHA models (Robert and Benedict) give good agreement with experimental data. Measurement error is too large to discriminate between these three models. The Luo model[4] overpredicts the thermal pressure.

The measured thermal expansion is shown in Fig. 7 between 20 and 80 GPa and compared with the models. The 300K values for the volume were determined from our experimental equation of state. At high temperature, the pressure varies by less than 1 GPa, which leads to the scatter of measured volume observed in Fig. 7. Apart from this scatter the data can be considered as isobaric. The expansion appears linear, consistent with the predictions of Song[7] that the coefficient of thermal expansion is temperature-independent above 15 GPa. However, the quantitative agreement at high temperature is also close to the two nonlinear QHA models (Robert, Benedict) in the temperature range over which we collected data.

The Luo model significantly deviates from the data. The apparent agreement with thermal expansion results of Gordon et al.[20] at high temperature which is shown in their report is due to an error in use of temperature units. Potential sources for this inconsistency include their use of the local density approximation (LDA) where the others used the generalized gradient approximation (GGA), and their apparent non-inclusion of zero-point effects in calculation of the thermal properties.

V. MELTING BEHAVIOUR

Melting curves of metals under pressure have been debated recently. The experimental melting lines of iron, as well as tantalum, molybdenum, and tungsten differ by up to 6000K around 300 GPa for the worst case, depending on the compression technique (static/dynamic)[47], but also the melting diagnostic. X-ray detection of melting[46,49], based on the measurement of the diffuse X-ray signal scattered by the liquid, has called into question the conventional optical detection of melting[47,52] in laser-heated diamond anvil cells. The new diagnostic leads to higher temperature melting points[51,53]. The XRD technique also allowed the observation of changes undergone in the laser-heated sample: thermal expansion, recrystallization from a fine powder to a few single crystals[46,51] - this phenomenon becoming faster with temperature increase[50] - but also unwanted chemical reactions between

TABLE III: Lattice parameters of beryllium as a function of T measured during several heating series in Be_3 and Be_4 samples. The pressure has been calculated using MgO volume with Ref. 26 EoS. 300 K values have been fixed at the value predicted by our equation of state for Be compressed in NaCl.

T (K)	MgO V(Å^3)	a(Å)	c (Å)	T (K)	MgO V(Å^3)	a (Å)	c (Å)
23.3(6) GPa				30(1) GPa			
300		2.164	3.414	300		2.139	3.380
1289	17.081	2.187	3.463	1595	16.764	2.173	3.415
1386	17.081	2.188	3.462	1670	16.686	2.175	3.416
1488	17.134	2.190	3.464	1927	16.813	2.173	3.422
1544	17.145	2.191	3.473	1929	16.782	2.176	3.424
1656	17.160	2.193	3.466	1926	16.816	2.177	3.424
1711	17.253	2.194	3.461	2021	16.872	2.173	3.465
1779	17.277	2.197	3.488	1489	16.694	2.166	3.406
1926	17.362	2.204	3.462	1457	16.734	2.165	3.405
2025	17.366	2.198	3.494	1400	16.639	2.165	3.407
				1355	16.667	2.165	3.408
45(3) GPa				59(1)GPa			
300		2.088	3.301	300		2.053	3.250
1440	15.763	2.114	3.341	1473	15.186	2.075	3.287
1496	15.771	2.115	3.343	1618	15.202	2.077	3.293
1566	15.777	2.116	3.345	1733	15.214	2.077	3.292
1643	15.808	2.117	3.338	1864	15.226	2.081	3.282
1707	15.814	2.119	3.349				
1773	15.801	2.118	3.350				
1850	15.818	2.119	3.360				
1970	15.858	2.122	3.352				
2029	15.818	2.124	3.345				
2106	15.899	2.124	3.356				
2083	15.858	2.125	3.336				
2156	15.865	2.123	3.351				
2403	15.966	2.129	3.363				
62.0(8) GPa				67.6(9) GPa			
300		2.044	3.238	300		2.034	3.222
1459	15.034	2.067	3.274	1517	14.823	2.052	3.242
1580	15.055	2.068	3.277	1638	14.841	2.053	3.257
1708	15.080	2.069	3.276	1771	14.862	2.055	3.254
1839	15.112	2.071	3.268	1884	14.882	2.055	3.248
1969	15.133	2.072	3.271	2003	14.919	2.054	3.269
2111	15.165	2.074	3.275	2139	14.926	2.059	3.256
2269	15.196	2.078	3.280	2273	14.985	2.061	3.260
76.3(6) GPa				82(1)GPa			
300		2.016	3.185	300		2.005	3.180
1554	14.517	2.037	3.221	1729	14.383	2.025	3.206
1661	14.506	2.037	3.222	1842	14.398	2.025	3.206
1773	14.537	2.038	3.220	1937	14.405	2.026	3.208
1882	14.551	2.039	3.222	2062	14.418	2.028	3.210
2002	14.562	2.040	3.231	2158	14.423	2.029	3.211
2129	14.601	2.043	3.217	2260	14.421	2.029	3.212
2129	14.616	2.044	3.220	2260	14.430	2.030	3.213
2317	14.646	2.045	3.214	2384	14.436	2.032	3.216
				2479	14.457	2.033	3.218
				2623	14.472	2.039	3.228

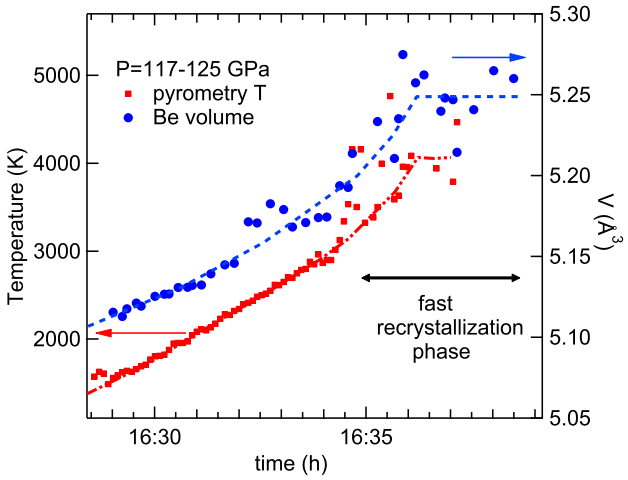

FIG. 9: (Color online) Evolution of pyrometry temperature and Be volume with time (and laser power) during one heating series for the Be_1 sample. The pressure from NaCl equation of state varied from 119 to 125 GPa. Fast recrystallization was observed between 3000K and 4000K, and resulted in unsteady temperature measurements (large scatter of the pyrometry temperature points). The dotted lines are guides to the eyes. The thermal expansion of beryllium stopped around 4000K which could be an indication of melting.

the sample and the pressure medium or the diamond anvil[51]. The onset of "fast recrystallization", evidenced by the appearance/disappearance of solid single crystal XRD spots on each XRD pattern, has been interpreted as a melting evidence[50]. Temperature plateaus, or decreases of in slope of the temperature rise as a function of time (and laser power) are also considered as melting evidences in a few studies[50,54].

In the case of beryllium, we have failed to record a diffuse X-ray scattered signal characteristic of a liquid phase even at moderate pressure - and therefore, with the largest samples - because of the low X-ray scattering cross section of Be. However, we did see qualitative effects such as "fast recrystallization" and changing temperature ramps which, in other studies, have been correlated with melting. "Fast recrystallization" corresponds to the appearance and disappearance of single-crystal spots on each subsequent collected diffraction pattern (every 8 seconds during the heating ramps). This phenomenon was observed over 400 K to 1000 K-wide temperature domains below the theoretical melting point of beryllium. It is also below the melting curve of the pressure transmitting medium, NaCl[48]. Fig. 8 presents the paths followed in phase space, with the regions where fast recrystallization was evident shown with red (filled) data points. The onset of fast recrystallization results in various changes in the temperature ramps such as jumps, plateaux, changes of T *vs.* time slopes or unsteady temperatures.

An example of the onset of unsteady temperature ramps during fast recrystallization can be seen in Fig. 9. In parallel, we show the evolution of the solid Be volume. Solid beryllium is observed and expands during the fast recrystallization sequence, indicating continued temperature increase. This is incompatible with the statement that the onset of fast recrystallization corresponds to melting made in earlier studies[50]: a solid sample cannot be brought to temperatures higher than its melting point. It can be noted in Fig. 9 that the solid beryllium stops expanding when the temperature reaches approximately 4000K. This could be a hint of melting - 4000K corresponds to the theoretical melting temperature. However, the data are too sparse to consider this volume plateau as a clear evidence, unlike the observation of the diffuse X-ray signal scattered by a liquid[46]. Fast recrystallization is likely to be caused by temperature-induced changes of the mechanical properties of the laser-heated solid metallic sample, such as mobility of grain boundaries. Our data on the onset of this phenomenon may be useful for benchmarking future models for mechanical properties of metals under pressure, or large scale atomistic models of the materials undergoing laser heating in a diamond anvil cell.

VI. CONCLUSION

The high pressure behavior of beryllium measured in this study has been compared with the predictions of state-of-the-art *ab initio* calculations published recently. The experimental cold compression curve of the hcp phase up to 191 GPa reveals a slight overestimation of bulk modulus under high pressure by the generalized gradient approximation[6,7]. The thermal expansion, predicted using *ab initio* phonon density of state and simple quasi-harmonic models[5,6], is in good agreement with measurements up to 82 GPa and 2600K. P-V-T data of hcp beryllium have been obtained in the 20-100 GPa and 300-2500K P-T range. They can be fitted by a quasi-harmonic model (Eqs. (2) and (3)) with the following parameters: $\theta^{(0)} = 949K$, V_{ref} =8.133 Å^3/atom, A=0.079 Å^{-3} and B=0.542. Agreement with theoretical models[5,6] demonstrates that Be exhibits the thermal behavior of a regular solid in this P-T range. The experimental EoS proposed here will be useful for its applications and for benchmarking future models. The hcp structure is seen to be remarkably stable. No sign of the bcc phase has been observed either at low or high pressure, which contradicts some reports[4,5]. Rapid recrystallization of the heated sample has been observed over a wide temperature range during heating cycles and shown not to be correlated with melting in this study; our observations do not contradict the predicted melting curve under pressure[5,6].

VII. ACKNOWLEDGEMENTS

We thank L. Benedict, T. Ogitsu and G. Robert for helpful discussion and comments. This work was performed on the ID30 and ID27 beamlines at the European Synchrotron Radiation Facility (ESRF), Grenoble, France. Sone of the work was performed under the auspices of the U.S. Department of Energy by Lawrence Livermore National Laboratory under Contract DE-AC52-07NA27344.

[1] S. W. Haan, J. D. Lindt, D. A. Callahan, et al., Phys. of Plasmas **18**, 051001 (2011).
[2] R. E. Olson, G. A. Rochau, O. L. Landen and R. J. Leeper, Phys. of Plasmas **18**, 032706 (2011).
[3] D. Swift, D. Paisley and M. Knudon, AIP Conf. Proc. **706**, 119 (2003).
[4] F. Luo, L.-C. Cai, X.-R. Chen, F.-Q. Jing and D. Alfe, J. of Appl. Phys. **111**, 053503 (2012).
[5] G. Robert, P. Legrand and S. Bernard, Phys. Rev. B **82**, 104118 (2010).
[6] L. X. Benedict, T. Ogitsu, A. Trave, C. J. Wu, P. A. Sterne and E. Schwegler, Phys. Rev. B **79**, 064106 (2009).
[7] H.-F. Song and H.-F. Liu, Phys. Rev. B **75**, 245126 (2007).
[8] A. J. Martin and A. Moore, J. Less Common Metals **1**, 85 (1959).
[9] C. W. F. T. Pistorius, Progress in Solid State Chemistry vol 1, ed J. O. McCaldin and G. Somorja (New York: Pergamon) (1976).
[10] M. Francois and M. Contre, in Conference Internationale sur la Metallurgie du Beryllium (Universite de France, Paris, Grenoble, 1965).
[11] L. C. Ming and M. H. Manghnani, J. Phys. F: Met. Phys. **14**, L1-L8 (1984).
[12] V. Vijayakumar, B. K. Godwal, Y. K. Vohra, S. K. Sikka and R. Chidambaram, J. Phys F: Met. Phys. **14**, 165 (1984).
[13] G. V. Sin'ko and N. A. Smirnov, Phys. Rev. B **71**, 214108 (2005).
[14] B. Palanivel, R. S. Rao, B. K. Godwal and S. K. Sikka, J. Phys.: Condens. Matter **12**, 8831 (2000).
[15] W. J. Evans, M. J. Lipp, H. Cynn, C.-S. Yoo, M. Somayazulu, D. Hausermann, G. Shen and V. Prakapenka, Phys. Rev. B **72**, 094113 (2005).
[16] K. Nakano, Y. Akahama and H. Kawamura, J. Phys.: Condens. Matter **14**, 10569 (2002).
[17] W. J. Evans et al., reported in 6, unpublished.
[18] M. Boivineau, L. Arles, J. M. Vermeulen and Th. Thevenin, International Journal of Thermophysics, **14**, 427 (1993).
[19] C. A. Swenson, J. Appl. Phys. **70**, 3046 (1991).
[20] P. Gordon, J. Appl. Phys. **20**, 908 (1949).
[21] P. Loubeyre, R. LeToullec, D. Hausermann, M. Hanfland, R. Hemley, H. Mao and L. Finger, Nature **383**, 702 (1996).
[22] A. Dewaele, P. Loubeyre and M. Mezouar, Phys. Rev. B **70**, 094112 (2004).
[23] P. Loubeyre, R. Le Toullec, M. Hanfland, L. Ulivi, F. Datchi and D. Hausermann, Phys. Rev. B **57**, 10403 (1998).
[24] T. Sakai, E. Ohtani, N. Hirao and Y. Ohishi, J. Appl. Phys. **109**, 084912 (2011).
[25] S. Ono, T. Kikegawa and Y. Ohishi, Sol. State Comm. **137**, 517 (2006).
[26] P. I. Dorogokupets and A. Dewaele, High Pressure Research **27**, 431 (2007).
[27] M. Mezouar, W. Crichton, S. Bauchau, F. Thurel, H. Witsch, F. Torrecillas, G. Blattmann, P. Marion, Y. Dabin, J. Chavanne, O. Hignette, C. Morawe, and C. Borel, J. Synchrotron Radiat. **12**, 659, (2005). E. Schultz et al., High Press. Res. 25, 71, 2005.
[28] L. R. Benedetti and P. Loubeyre, High Pressure Research **24**, 423 (2004).
[29] N. Velisavljevic, G. N. Chestnut, Y. K. Vohra, S. T. Weir, V. Malba and J. Akella, Phys. Rev. B **65**, 172107 (2002).
[30] U. Haussermann and S. I. Simak, Phys. Rev. B 64, 245114 (2001).
[31] P. Vinet, J. R. Smith, J. Ferrante and J. H. Rose, Phys. Rev. B **35**, 1945 (1987).
[32] J. F. Smith and C. L. Arbogast, J. Appl. Phys. **31**, 99 (1960).
[33] D. J. Silversmith and B. L. Averbach, Phys. Rev. B **1**, 567 (1970).
[34] L. Testardi and J. Condon, Phys. Rev. B **1**, 3928 (1970).
[35] A. Migliori, H. Lebbetter, D. J. Thomas and T. W. Darling, J. Appl. Phys. **95**, 2436 (2004).
[36] J. P. Perdew and A. Zunger, Phys. Rev. B **23**, 5048 (1981).
[37] J. P. Perdew, K. Burke and M. Ernzerhof, Phys. Rev. Lett. textbf77, 3865 (1996).
[38] L. Hedin and B. I. Lundqvist, J. Phys. C **4**, 2064 (1971).
[39] J. P. Perdew, J. A. Chevary, S. H. Vosko, K. A. Jackson, M. R. Pederson, D. J. Singh, and C Fiolhais, Phys. Rev. B **46**, 6671 (1992).
[40] O. L. Anderson, D. G. Isaak and S. Yamamoto, J. Appl. Phys. **65**, 1534 (1989).
[41] P. I. Dorogokupets and A. R. Oganov, Phys. Rev. B **75**, 024115 (2007).
[42] K. Takemura and A. Dewaele, Phys. Rev. B **78**, 104119 (2008).
[43] L. X. Benedict, private communication (2011).
[44] A. Dewaele, M. Torrent, P. Loubeyre and M. Mezouar, Phys. Rev. B **78**, 104102 (2008).
[45] O. L. Anderson, Physics of the Earth and Planetary Interiors **112**, 267 (1999).
[46] A. Dewaele, M. Mezouar, N. Guignot and P. Loubeyre, Phys. Rev. B **76**, 144106 (2007).
[47] D. Errandonea, B. Schwager, R. Ditz, C. Gessmann, R. Boehler and M. Ross, Phys. Rev. B **63**, 132104 (2001).
[48] R. Boehler, M. Ross and D. B. Boercker, Phys. Rev. Lett. 78, 4589 (1997).
[49] G. Shen, V. B. Prakapenka, M. L. Rivers and S. R. Sutton, Phys. Rev. Lett. **92**, 185701 (2004).
[50] R. Boehler, D. Santamaria-Perez, D. Errandonea and M. Mezouar, J. Phys. Conf. Ser. **121**, 022018 (2008).
[51] A. Dewaele, M. Mezouar, N. Guignot and P. Loubeyre, Phys. Rev. Lett. **104**, 255701 (2010).
[52] R. Boehler, Nature **363**, 534 (1993).
[53] G. Morard et al., Phys. Chem. Miner. **38**, 767 (2011).
[54] O. T. Lord, M.J. Walter, R. Dasgupta, D. Walker and S.M. Clark, Earth Planet. Sci. Lett. **284**, 157 (2009).